Reconstructing the Blood Pressure Waveform using a Wearable Photoplethysmograph Sensor and Hydrostatic Pressure Variations Measured by Accelerometers

by

Aleksandar Marinković

B.Sc. Mechanical Engineering
University of Kragujevac, Serbia (2002)

Submitted to the Department of Mechanical Engineering
in Partial Fulfillment of the Requirements for the Degrees of

Master of Science in Mechanical Engineering

at the

Massachusetts Institute of Technology

February 2007

Signature of Author _____
Aleksandar Marinković
Department of Mechanical Engineering
January 12, 2007

Certified by _____
Haruhiko H. Asada
Professor of Mechanical Engineering
Thesis Supervisor

Accepted by _____
Lallit Anand
Professor of Mechanical Engineering
Chairman, Department Committee on Graduate Students

Reconstructing the Blood Pressure Waveform using a Wearable Photoplethysmograph Sensor and Hydrostatic Pressure Variations Measured by Accelerometers

by

Aleksandar Marinković

Submitted to the Department of Mechanical Engineering
on January 12, 2007 in partial fulfillment of the requirements
for the Degrees of Master of Science in Mechanical Engineering

ABSTRACT

An important part of a routine clinical examination is the assessment of the arterial blood pressure waveform. The variations in shape of the waveform indicate the presence of disease.

In this work, a method is developed for the reconstruction of arterial blood pressure waveform using the signals obtained from a noninvasive wearable photoplethysmographic Ring Sensor and hydrostatic pressure variations measured by an Arm Accelerometer Sensor. A dynamic model with the Wiener model structure is used to establish the relationship between transmural pressure and photoplethysmographic signal. Tuned nonlinear dynamic model has been shown to be capable of estimating the arterial blood pressure waveform. The algorithm has been applied to experimental blood pressure measurements in a healthy subject and shown to provide accurate waveform reconstruction. As a result, the use of a wearable photoplethysmographic Ring Sensor can be extended to provide a finger arterial blood pressure waveform.

Thesis Supervisor: Haruhiko Harry Asada
Title: Ford Professor of Mechanical Engineering

TO MY FAMILY

Acknowledgments

I wish to thank my wife, Marina, whose support has carried me through all those long days and late nights. I wish to thank my parents, Milan and Goca, and my sister, Aleksandra, for their support throughout the years of my academic endeavors. I wish also to thank Prof. Asada whose guidance made this work attainable. Finally, thanks to all of my lab mates from whom I learned a lot and whose companionship I enjoyed very much.

Table of Contents

Table of Figures

1 Introduction

1.1 Arterial Blood Pressure Measurements

It is a hard and challenging task to quantify arterial blood pressure (ABP) in the human circulatory system. The branching network of blood vessels creates a structure that exhibits both lumped and distributed dynamic behavior. The time varying attribute of circulation additionally increases the system's complexity. As a result, the measurements of blood pressure are not static but undergo natural variations from one heartbeat to another, throughout the day (in a circadian rhythm), and in response to many factors such as disease and stress [1].

Blood pressure is defined as the pressure exerted by the blood against blood vessel's wall and comes from two forces: one is the force created by the heart as it pumps blood into the vessels and through the circulatory system, and the other is the force of the vessels as they resist the blood flow. Usually, blood pressure refers to systemic arterial blood pressure, i.e., the pressure in the large arteries delivering blood to body parts other than lungs. The peak pressure in the arteries during the cardiac cycle is defined as the systolic pressure; the lowest pressure is the diastolic pressure. The mean arterial pressure and pulse pressure are other important quantities. Typical values for a resting, healthy adult human are approximately 120 mmHg systolic and 80 mmHg diastolic (written as 120/80 mmHg), with large individual variations.

The most accurate measurements of blood pressure are done invasively by placing a flexible tube, cannula, into a blood vessel and connecting it to an electronic pressure transducer. This technique is regularly employed in intensive care medicine and for

research purposes. However, this invasive technique is unpleasant and painful for the patient and it is associated with complications such as infection and bleeding. Therefore, simpler and quicker noninvasive techniques are more commonly used for routine examinations and for monitoring of ABP but at the cost of being less accurate.

Noninvasive blood pressure measurements utilize the auscultatory and the oscillometric methods. With the auscultatory methods the blood pressure is manually measured using a stethoscope and sphygmomanometer, an inflatable cuff placed around the upper arm at the heart level attached to a manometer. The examiner inflates the cuff until the artery is completely occluded and then slowly releases the pressure in the cuff. When blood flow begins again in the brachial artery the first Korotkoff sound can be heard with a stethoscope. The cuff pressure at that instant shows the systolic blood pressure. The cuff pressure is further released until no sound can be heard. The pressure in the cuff corresponding to the last, fifth, Korotkoff sound is equal to the diastolic blood pressure.

The oscillometric methods are very similar to the auscultatory methods. The main difference is that instead of using a stethoscope to detect blood flow there is an electronic pressure sensor (transducer) fitted in the cuff. The cuff is placed on the upper arm and automatically inflated by an electric pump. When pressure in the cuff measured with a pressure transducer is gradually released, the small oscillations in cuff pressure caused by the cyclic expansion of the brachial artery are recorded and used to calculate systolic and diastolic pressures.

Oscillometric measurement requires less skill than the auscultatory measurement, and may be suitable for use by non-trained staff and for automated patient monitoring.

However, these noninvasive techniques are limited to discrete blood pressure measurements; that is to say, they only estimate systolic and diastolic pressures, not the entire blood pressure waveform.

1.2 Motivation

Nowadays, an important part of a routine clinical examination is the assessment of the arterial pulse pressure. It is well known that changes in the character of blood pressure waveform indicate the presence of disease. However, when the mercury sphygmomanometer was developed clinicians began to concentrate exclusively on the absolute values of systolic and diastolic blood pressure rather than on the shape of the waveform, in that way, disregarding important qualitative information in favor of information covering only the extremes of pressure.

Why is it important to know the shape of the waveform? The systolic upstroke or anacrotic limb mainly reflects the pressure pulse produced by left ventricular contraction. The pressure pulse is followed slightly later by the flow wave caused by the actual displacement of blood volume. The anacrotic shoulder, that is, the rounded part at the top of the waveform, reflects primarily volume displacement. The peak of the waveform is assigned as systolic pressure. The dicrotic limb is demarcated by the dicrotic notch, representing closure of the aortic valve and subsequent retrograde flow. The location of the dicrotic notch varies according to the timing of aortic closure in the cardiac cycle. For example, in some diseases such as hypovolemia aortic closure is delayed. Consequently, the dicrotic notch occurs farther down on the dicrotic limb in hypovolemic patients. Also, the dicrotic notch position on the dicrotic part of the waveform depends

on the site in the arterial tree where the ABP is measured. The shape and proportion of the diastolic runoff wave that follows the dicrotic notch change with arterial compliance and heart rate. The bottom of the blood pressure waveform is known as the diastolic pressure.

In some diseases such as in hypertension, which is due to age-related arterial stiffening, atherosclerotic narrowing, or rennin related vasoconstriction, an increased magnitude of reflected waves which fuse with the systolic upstroke results in a high pulse pressure and late high systolic peak [2], often manifested as a narrow systolic peak in the peripheral ABP waveform tracing [3].

The shape of the waveform contains much more information than the current noninvasive blood pressure measurements. These measurements are limited to the simple discrete assessments of systolic and diastolic blood pressures. Because of that, our goal here is to develop a general methodology for estimating the ABP waveform using measurement from a noninvasive device such as finger photoplethysmograph (PPG) and measurement of hydrostatic pressure variations assessed from accelerometers.

1.3 Document Layout

This thesis is organized as follows: Chapter 2 describes the pressure-volume, or more precisely the pressure-photoplethysmograph, relationship in arteries and how it can be modeled as a combination of a linear dynamic model with a static nonlinearity on the output, known as Wiener model structure. Chapter 3 presents a parameter identification method with particular emphasis on the numerical procedure for identification of parameters of a nonlinear model. Chapter 4 highlights biosensors, describing those used

in our experiments. Chapter 5 describes the experimental setup and the protocol followed to obtain validation data from human subjects. In Chapter 6, experimental data are presented demonstrating the feasibility of Wiener model structure for the reconstruction of arterial blood pressure waveform from the signals coming from a wearable Ring Sensor. Finally, concluding remarks and suggestions for future work are given in Chapter 7.

2 Transmural Pressure-Volume Relationship in Arteries

To estimate the arterial blood pressure from noninvasive photoplethismographic measurements a model relating the blood pressure to arterial volume changes is needed. Before choosing the model, we will focus first on the arterial wall, presenting its viscoelasticity based on structure, and then, we will introduce the nonlinearity of the pressure-volume characteristics. Finally, transmural pressure (P_{tm}) can be altered either by changing internal or external pressure acting on the arterial wall. We have chosen to change the internal pressure by altering the hydrostatic pressure.

2.1 Nonlinear Viscoelasticity of Arterial Wall

Blood vessels belong to the class of soft tissues [4]. They exhibit the nonlinearity in stress-strain relationship and hysteresis when subjected to cyclic loading. They also creep under constant stress and relax under constant strain. It is to be expected that these mechanical properties have a molecular structural basis. However, the mechanical properties depend not only on vessel's composition, structure, and ultrastructure, but also how the different constitutive elements interplay. The complexity of composition and structure is known through chemical and histological studies. On the contrary, how those parts cooperate and synergize is much harder to understand.

2.1.1 Viscoelasticity of Arterial Wall

In order to formulate a mechanical model of arterial wall we shall first describe briefly its content and structure. Arteries are the blood vessels that carry blood from the heart to the body. There are several types of arteries in the body and their structure slightly differs along the arterial tree. In general, the arterial wall consists of three layers: intima, media, and adventitia. These three layers are divided with elastic membranes. The relative ratio of the layers and their structure depend on the site in the arterial tree [5]. The intima consists of the endothelial cells, the basement membrane, and a layer composed of an aggregation of collagen, elastin, smooth muscle and other cells. The media consists of smooth muscle in concentric layers tied to a structure by elastin and collagen fibers. In smaller arteries the elastin is less prominent in the media, and the smooth muscle fibers increase in amount. Finally, the adventitia is a loosely organized connective tissue.

The mechanical properties of each of the structural parts are very different [4]. Elastin by itself has a low elastic modulus, a very small hysteresis loop in cyclic loading and little stress relaxation. Collagen has more than three orders of magnitude larger elastic modulus than elastin, a moderate stress relaxation, a moderate hysteresis loop, and a high stress response at small deformation. Finally, smooth muscle has the smallest elastic modulus, an order of magnitude smaller than elastin, a very prominent hysteresis loop in cyclic loading, but lower stress response comparing to elastin and collagen.

Unsurprisingly, the resulting behavior of a material consisting of components having such diverse properties will not depend only on the composition, but also on the structure. Subjected to a relaxation test the structure does not relax with a single

relaxation time [6]. The segments of varying length contribute to the relaxation, with the simpler and shorter segments relaxing much more quickly than the long ones. This will result in a distribution of relaxation times, which in turn produces a relaxation spread over a much longer time than can be modeled accurately with a single relaxation time. From engineering prospective this can be approximated with spring-dashpot elements combined into the Maxwell-Weichert model (Fig. 1).

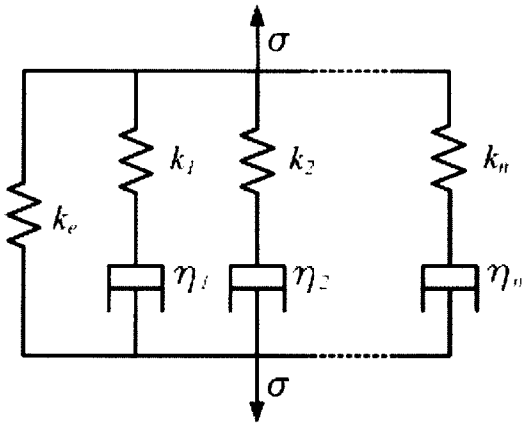

Figure 1. Viscoelastic Maxwell-Weichert model

Under assumption that the spring-dashpot elements are linearly involved, the stress-strain relationship obtained from a Maxwell-Weichert model can be written as

$$\bar{\sigma} = \left\{ k_e + \sum_{i=1}^{n} \frac{k_i s}{s + \frac{1}{\tau_i}} \right\} \bar{\varepsilon} \tag{2.1}$$

where $\bar{\sigma}$ and $\bar{\varepsilon}$ are Laplace transforms of the total stress and total strain, respectively, k_e and k_i are the Young's moduli of different "spring" elements, and $\tau_i = \frac{\eta_i}{k_i}$ are the time constants corresponding to each of the spring-dashpot pairs.

For the purpose of this work we will use a Maxwell-Weichert model representing the three major constituents of arterial wall; elastin, collagen, and smooth muscle. We will assume that elastin can be represented as a spring-like element with modulus k_e, and collagen and smooth muscle as spring-dashpot combinations (Fig. 2).

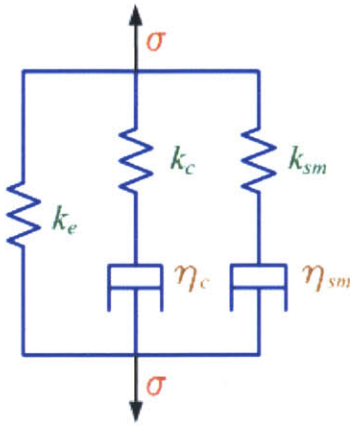

Figure 2. Maxwell-Weichert lumped parameter model representing arterial wall

Stress-strain relationship of such a linear model can be written in complex domain as:

$$\bar{\sigma} = \left\{ k_e + \frac{k_c s}{s + \frac{1}{\tau_c}} + \frac{k_{sm} s}{s + \frac{1}{\tau_{sm}}} \right\} \bar{\varepsilon} \qquad (2.2)$$

where $\tau_c = \frac{\eta_c}{k_c}$ and $\tau_{sm} = \frac{\eta_{sm}}{k_{sm}}$ are the relaxation time constants corresponding to collagen and smooth muscle, respectively.

2.1.2 Nonlinear Arterial Wall Dynamics

It has been shown in [7] that the pressure-volume relationship in human finger artery is nonlinear and dynamic, and that relaxed artery collapses at near-zero transmural pressure. In the same report it was obvious that hysteresis was present, which lead the authors to reason that a precise unstressed artery diameter does not exist, but depends on whether the artery is observed during the cuff inflation or deflation.

The dynamic unloading of the finger arterial walls is the basic principle of the volume-clamp blood pressure measurement method [8, 9], by means of a servo system keeping the arterial wall at zero transmural pressure, i.e. at the arterial unstressed volume. Then, in order to provide an objective criteria for an adjustment algorithm used in an instrument utilizing the method the pressure-volume (i.e. transmural pressure-photoplethismograph) relationship of human finger artery is required [7]. This relationship should be known both quasi-statically and dynamically, because the position of the servo set point on the curve is of especial importance (Fig. 3).

Here, we propose that the transmural pressure-volume relationship can be described as nonlinear dynamic viscoelastic.

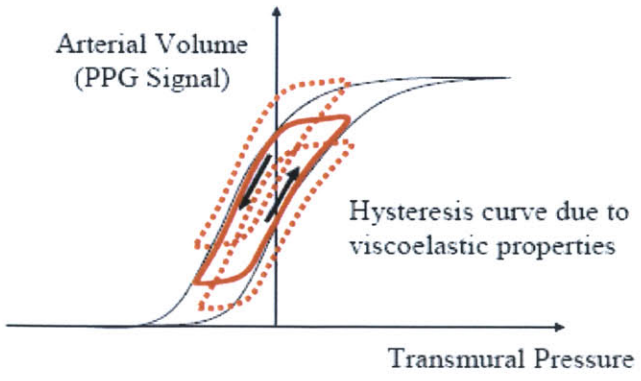

Figure 3. Dynamical nature of arterial pressure-volume curve

2.2 Varying Transmural Pressure by Altering Intravascular Hydrostatic Pressure

As we mentioned previously, transmural pressure can be altered either changing internal or external pressure acting on the arterial wall. We chose to change the internal pressure by altering the hydrostatic pressure.

If one keeps the arm at the heart level and measures ABP, one gets P_{heart}. If then one moves the arm below or above the heart and repeats the measurement, using Pascal's principle, one gets a new ABP, P_{ABP}. The new P_{ABP} is related with the ABP measured at the heart level by the hydrostatic pressure, P_{hyd}. This can be written as:

$$P_{ABP} = P_{heart} + P_{hyd} = P_{heart} - \rho g h \tag{2.3}$$

where ρ is the density of the blood (1050 – 1060 kg/m^3), g is the acceleration due to gravity, and h is the height relative to the heart level. In Eq. 2.3 we have chosen that the value of h will be negative if the measurement site is below the heart level, and positive if it is above the heart level.

By definition, the transmural pressure, P_{tm}, in a site at heart level can be stated as:

$$P_{tm} = P_{heart} - P_{external} \tag{2.4}$$

where $P_{external}$ is the pressure applied externally by a cuff.

Figure 4 schematically depicts previous relation, in addition to showing the stress balance in arterial wall.

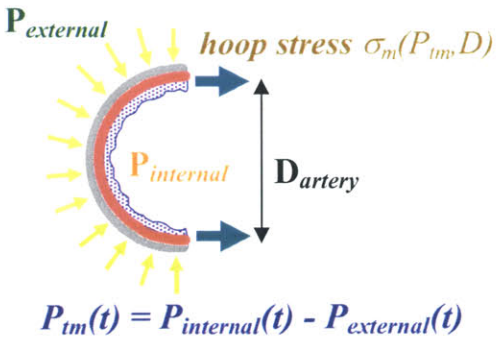

Figure 4. Pressure balance in arterial wall: $P_{tm}(t)$ - transmural pressure, $P_{int\,ernal}(t)$ - intra-arterial pressure, $P_{external}(t)$ - externally applied pressure; $\sigma_m(P_{tm}, D)$ - stress in arterial wall

Combining Eqs. 2.3 and 2.4 , the transmural pressure can be written as:

$$P_{tm} = P_{ABP} + \rho g h - P_{external} \tag{2.5}$$

According to Eq. 2.5, it is logical to conclude that transmural pressure can be changed by varying the height of the measurement site relative to the heart level. That allows us to "scan" a region of transmural pressure values depending on $\pm \rho g h_{max}$ (h_{max} is the maximum achievable height that depends on subject's arm length) and applied external pressure. Because we are mostly interested in the transmural pressure values around zero (the artery is then the most compliant), it is recommended to apply an external pressure close to the mean arterial pressure at the heart level. This principle will allow us to record the P_{tm} *-PPG* curve experimentally by changing the arm position. We will show later how the hydrostatic pressure can be measured simply by reading the outputs of two accelerometers and using a kinematic relationship.

3 Nonlinear System Identification

After choosing a model describing a nonlinear P_{tm}-PPG dynamic relationship in finger arteries, the next step is to identify the parameters of the model. In this section, we will explain our approach to address this problem.

In the past, modeling was mainly restricted to linear (or almost linear) systems for which an analytical treatment is possible. In recent years, there has been a tremendous progress in the methodology of system identification particularly in control engineering. The availability of modern estimation theory and sophisticated computational algorithms has contributed to the rapid growth of system identification technology. Now it is possible to tackle, to some extent, nonlinear systems. After all, nonlinearity is at the heart of most of the interesting dynamics. One of the major difficulties in dealing with these systems is the lack of unified mathematical theory for representing nonlinear system characteristics. Unless we impose a specific system representation in advance it is not practical to talk about identification of nonlinear systems.

The pressure-volume relationship in human finger artery that is nonlinear and dynamic can often be well described as a combination of a linear system and a static nonlinearity. Here, we will focus on a particular class of nonlinear systems known as the Wiener systems.

3.1 The Wiener Model

A number of nonbiological and biological examples can be found in literature of systems with a nonlinear relationship between the input and output sequences [10].

Often, that relationship can be well described by a combination of a linear system followed by nonlinearity, known as nonlinear Wiener model.

A Wiener model is depicted in Figure 5. It consists of a linear dynamic system $H(q)$ followed by a static nonlinearity f. The input u and the output y are measurable, possibly with noise, but we cannot measure the intermediate signal x.

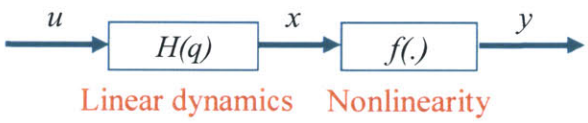

Figure 5. Wiener model structure

Our goal is to find a linear dynamic model relating u and x, and a nonlinear static model relating x and y. Moreover, we will consider parametric models, where the output can be described as a function of the input and some other parameters. Different values of these parameters will describe different models. For the linear dynamic system relating $u(t)$ with $x(t)$ in discrete time we can write:

$$x(t) = H(q,\theta)u(t) \tag{3.1}$$

where q is the time-shift operator and θ is a parameter vector describing linear system. The nonlinear system relating $x(t)$ with $y(t)$ is described as:

$$y(t) = f(x(t),\eta) \tag{3.2}$$

where f is nonlinear function of $x(t)$ and the parameters η. Using measurements $u(t)$ and $y(t)$ we want to estimate the parameters θ and η.

For given values of the parameters θ and η, and an input u we can calculate the predicted output, $\hat{y}$. This predicted output, $\hat{y}(t,\theta,\eta)$, will depend on the parameters, as well as the time t.

The quality of the estimate is measured by mean squared error criterion:

$$V_N(\theta,\eta)=\frac{1}{N}\sum_{t=1}^{N}(y(t)-\hat{y}(t,\theta,\eta))^2 \tag{3.3}$$

where $y(t)$ is the measured output, and N is the number of data points. The resulting optimization problem is solved when the values of θ and η that minimize previous criterion are found.

For a chosen model structure and the given measurements, $V_N(\theta,\eta)$ may be formed explicitly as a function of parameters θ and η. If it is too complicated to minimize the criterion analytically, numerical methods could be used. In that case, it is necessary to provide an initial guess of the parameter values. We will suggest a way to make an initial estimate.

3.2 Optimization Method

In general, the function given in Eq. 3.3 can be minimized numerically. The extensive literature on such numerical problems exists[11-13].

Assuming that we have an initial estimate of θ and η, to calculate better estimates that lower the value of the prediction error criterion, Eq. 3.3, the following iterative scheme can be used:

$$\hat{w}^{(i+1)}=\hat{w}^{(i)}+\alpha_i h^{(i)} \tag{3.4}$$

where $\hat{w}^{(i)} = \begin{pmatrix} \hat{\theta} \\ \hat{\eta} \end{pmatrix}^{(i)}$, $h^{(i)}$ is a search direction and α_i *is* a positive constant determined to ensure that the value of $V_N(\theta,\eta)$ is decreased in each iteration step (i is iteration number). If the search direction is selected in a proper way we can guarantee convergence to a local minimum of the criterion to be minimized. A typical minimization method using values of the function $V_N(\theta,\eta)$ and its gradient is Gauss-Newton method. This method uses the search direction given by:

$$h^{(i)} = \left[G_N\left(\theta^{(i)},\eta^{(i)}\right)\right]^{-1} V_N'\left(\theta^{(i)},\eta^{(i)}\right) \tag{3.5}$$

with the Hessian given by:

$$G_N(\theta,\eta) = \frac{1}{N}\sum_{t=1}^{N}\Psi(t,\theta,\eta)\Psi^T(t,\theta,\eta) \tag{3.6}$$

and the criterion gradient:

$$V_N'(\theta,\eta) = -\frac{1}{N}\sum_{t=1}^{N}\Psi(t,\theta,\eta)\varepsilon(t,\theta,\eta) \tag{3.7}$$

where Ψ is the gradient matrix of $\hat{y}$ with respect to θ and η, and ε is the prediction error.

If the prediction errors are independent the Gauss-Newton search direction is given by:

$$h^{(i)} = -\left[\frac{1}{N}\sum_{t=1}^{N}\Psi(t,\theta,\eta)\Psi^T(t,\theta,\eta)\right]^{-1}\frac{1}{N}\sum_{t=1}^{N}\Psi(t,\theta,\eta)\varepsilon(t,\theta,\eta) \tag{3.8}$$

what is the least square solution of overdetermined system of equations:

$$\Psi^T(t,\theta,\eta)h^{(i)} = \varepsilon(t,\theta,\eta), \quad t = \overline{1,N} \tag{3.9}$$

The problem of finding $h^{(i)}$ in Eq. 3.9 can be solved using QR factorization [14]. The condition for using this method is that involved functions must be differentiable.

It is important to note that the local minima problem of the squared error criterion can be handled by trying several different initial parameter estimates, or making the first parameter estimate so accurate that the criterion converges to the global minimum. It has been suggested [15] to start with a linear model and then augment it to a nonlinear structure.

3.3 Consistency

If the system is given with Eq. 3.2 the goal of parameter estimation is to find true parameter values θ_0 and η_0. That means, if we apply a parameter estimation method to data $\{u(t), y(t)\}$ coming from the system, we want the estimated values of θ and η to be equal to the true values θ_0 and η_0. For such an estimate is said to be consistent.

Definition (Consistency): Assume that the true system is given by the parameters θ_0 and η_0. Let θ_N and η_N denote the estimates obtained from a data set containing N data pairs. The estimate is said to be consistent if $\theta_N \to \theta_0$ and $\eta_N \to \eta_0$ when $N \to \infty$.

The question of consistency of parameter estimates is not trivial [14]. Because the prediction error criterion may have several local minima, the estimates obtained from one of these minima will not be consistent in general. The parameter estimates are consistent if the following theorem is satisfied. The proof of the theorem can be found in [14].

Theorem: Suppose that the true system is described by:

$$y(t) = f(H(q,\theta_0)u(t),\eta_0) \tag{3.10}$$

Assuming that the linear system H is stable, that the nonlinear function $f(.,\eta)$ is differentiable with a first derivative uniformly continuous on the set of real numbers $\mathbf{R}$, and that:

1. The linear model structure is globally identifiable [13]
2. The input data set is informative enough [13]
3. The input to the nonlinearity, $\{x(t)\}_{t=1}^{N}$, is dense on $\mathbf{R}$ when N tends to infinity [14].
4. The number of parameters in the initial estimate, n_θ and n_η, as well as the number of data points, N, tends to infinity in such a way that

$$\frac{n_\theta}{N} \to 0 \text{ and } \frac{n_\eta}{N} \to 0 \tag{3.11}$$

where n_θ is the number of parameters in H, and n_η is the number of parameters in f.

Then, obtained parameter estimates $\hat{\theta}$ and $\hat{\eta}$ minimizing $V_N(\theta,\eta)$ in Eq. 3.3 are consistent. The consistency here excludes a constant gain that can be arbitrarily distributed between the linear and nonlinear subsystem.

4 Wearable Biosensors

Minimally invasive and noninvasive biosensors have received growing medical interest [16] because of their increasing reliability and richness of real-time information that they provide. Several wearable sensors exist in the market to measure "vital signs", such as heart rate, arterial blood pressure, oxygen saturation, temperature, and respiration rate. In particular, in ambulatory blood pressure measurements the most standard devices are portable oscillometric monitors. These devices have two main limitations: on the one side, they provide, in most of the cases, just particular points on the blood pressure waveform such as systolic and diastolic blood pressures, and on the other, they require motionless state of the subject during measurement [17]. Attempts to overcome the first limitation are made with devices such as Finapres, Portapres, or Finometer (Finapres Medical Systems, The Nederlands) [18, 19], which are capable to continuously measure ABP for over 60 hours. However, these devices are fairly big, certainly not wearable, and too expensive for using outside laboratories or hospitals. Because of these limitations, our goal has been to develop a methodology necessary for transforming the signals from a wearable photoplethysmographic Ring Sensor and a wearable Arm Accelerometer Sensor to a continuous ABP waveform. Here, we will first describe both sensors. Then, we will explain briefly the Finapres sensor (Ohmeda 2300) against which we compare our measurements.

4.1 Wearable Photoplethysmographic Ring Sensor for Blood Pressure Measurements

The plethysmograph, known in Italian as a "pletismografo", was invented by Angelo Mosso of Turin around 1870 [20]. It was first described in Scientific American in 1872, and used initially in scientific studies of emotions, as well as in criminal interrogations. Today, a modern version of the plethysmograph sensor is the photoplethysmograph, an optical device utilizing light absorption by the blood and tissue components.

The change in blood volume caused by the pressure pulse in artery is registered by illuminating the skin with light from a light emitting diode (LED), and then measuring the amount of light reflected, or transmitted, to a photodiode [21]. The volume, corresponding to the arterial diameter, is dynamically determined at any instant by the balance between the physiological arterial smooth muscle load and the arterial wall stress [22].

The basic concept of photoplethysmography has been incorporated into the Ring Sensor [23], a finger based device that comprises recent advances in the fields of optics and IC microelectronics. Figure 6 shows a conceptual diagram of an early Ring Sensor design [24, 25]. This sensor consisted of several optoelectronic components (photodiodes and LEDs), a central processing unit (CPU), a radio-frequency (RF) transmitter, a battery, and a ring chassis. The photodiodes detect the light sent from a LED that corresponds to the blood volume change in the patient's digital artery. The CPU controls the LED lighting sequence as well as the data acquisition and transmission

process. These signals are locally processed by an on-board CPU and transmitted to a host computer for diagnosis of the patient's cardiovascular conditions.

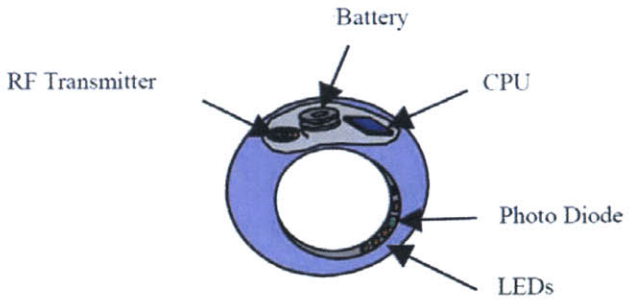

Figure 6. Conceptual diagram of Ring Sensor (from Rhee [23]).

For the purpose of our experimentation we adapted and improved this early Ring Sensor version. The power supply is now from an external power source, not from a battery, giving the stable voltage level necessary for longer experimental procedure. The CPU and RF transmitter are replaced by a 16-bit data acquisition card that is part of a personal computer. This improvement adds the flexibility in applying algorithms for different experimental protocols, the easiness in performing debugging procedures, and the significant increase in data transmission bandwidth. Furthermore, a pressure sensor is added into the Ring Sensor body to provide continuous information about the pressure applied to the finger.

4.2 Accelerometer Sensors for Hydrostatic Pressure Measurements

The accelerometers can be used to measure the tilt of an object. Tilt is a static measurement where gravity is the acceleration being measured. To achieve the highest resolution degree of a tilt measurement, a low-*g* and high-sensitivity accelerometer is

required. We used MEMSIC MXA2500G, ultra low noise ±1.7 *g* dual axis accelerometers with absolute outputs. These devices provide a sensitivity of 500mV/g in 5V applications. Their operation is based on heat transfer by natural convection and works like other accelerometers having a proof mass. The proof mass in the sensor is a gas. A single heat source, centered in the silicon chip is suspended across a cavity. Equally spaced aluminum/polysilicon thermopiles (groups of thermocouples) are located equidistantly on all four sides of the heat source (dual axis). Under zero acceleration, a temperature gradient is symmetrical about the heat source, so that the temperature is the same at all four thermopiles, causing them to output the same voltage. Acceleration in any direction will disturb the temperature profile, due to free convection heat transfer, causing it to be asymmetrical. The temperature, and hence voltage output of the four thermopiles will be different. The differential voltage at the thermopile outputs is directly proportional to the acceleration. There are two identical acceleration signal paths on the accelerometer, one to measure acceleration in the x-axis and the other to measure acceleration in the y-axis (Fig. 7). The device will experience acceleration in the range of +1 *g* to -1 *g* as the device is tilted from -90 degrees to +90 degrees respectively (1 *g* = 9.8 m/s).

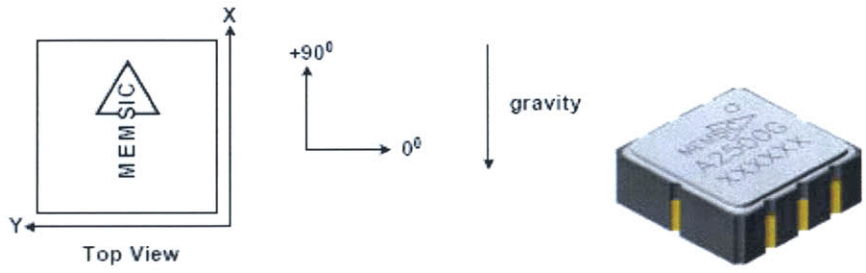

Figure 7. Accelerometer's sensing directions: The MEMSIC logo's arrow indicates the +X sensing direction of the device. The +Y sensing direction is rotated 90° away from the +X direction following the right-hand rule.

An accelerometer is most sensitive to changes in tilt when the accelerometer's sensitive axis is perpendicular to the force of gravity, or parallel to the Earth's surface. Similarly, when the accelerometer's axis is parallel to the force of gravity (perpendicular to the Earth's surface), it is least sensitive to changes in tilt. When one axis has a small change in output per degree of tilt, then the second axis has a larger change in output per degree of tilt. The complementary nature of two signals obtained from perpendicular axes permits low cost accuracy in tilt sensing to be achieved.

In our application, it is necessary to know the height of the Ring Sensor relative to the heart. To measure the height accurately we have to use two accelerometers, one attached to the upper arm at the same height as the heart, and the other mounted on the Ring Sensor at the finger base [26]. The direction of the X-axis in both accelerometers is aligned with the longitudinal directions of the upper arm and the forearm, respectively (see Fig. 8). To known the lengths l_1 and l_2, defined in Figure 8, the height of the Ring Sensor from the heart is given by:

$$h = l_1 \cdot sin\theta_1 + l_2 \cdot sin\theta_2 \tag{4.1}$$

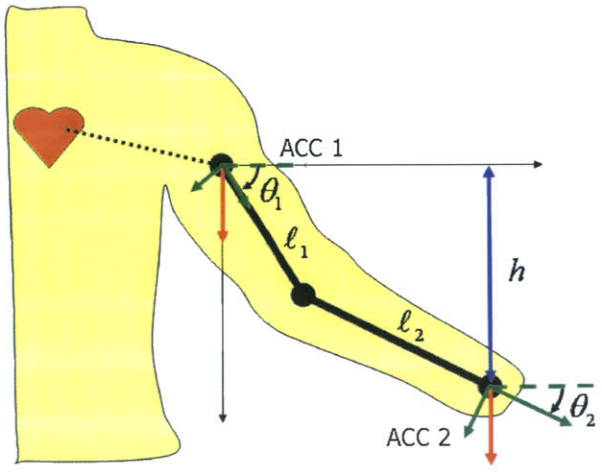

Figure 8. A height sensor using accelerometers

The use of height sensor for estimating hydrostatic pressure variations is straightforward. If the sensor position is below or above the heart level, the hydrostatic pressure, P_{hyd}, relative to the heart level can be written as:

$$P_{hyd} = -\rho g h \tag{4.2}$$

where ρ is the density of the blood, g the acceleration due to gravity, and h is the sensor height obtained from Eq. 4.1. If we measure the angles θ_1 and θ_2 relative to the horizontal arm position (X-axis reading from an accelerometer will be zero if the arm is in horizontal position) the expression in Eq. 4.1 says that the value of h will be negative if the sensor position is below the heart level, and positive if the sensor is placed above the heart.

4.3 Standard Reference for Continuous Blood Pressure Measurements

Finapres (Ohmeda 2300) is a noninvasive continuous finger ABP monitor based on the vascular unloading technique from Peñáz [8] and the physiological criteria from Wesseling [22]. With the volume-clamp method of Peñáz, although intra-arterial pressure changes continuously, the finger arteries are held at a fixed diameter by applying an external pulsating pressure via an inflatable finger cuff and a fast servo system. The setpoint is determined by the criteria of Wesseling [22]. The diameter at which the finger arteries are clamped is determined from an infrared plethysmograph mounted in the finger cuff, such that transmural pressure is zero and intra-arterial and cuff pressures are equal, both in shape and in level at all times.

There are numerous studies demonstrating the reliability of Finapres blood pressure measurements, mostly comparing them with the blood pressure measured in the brachial artery, which is a widely accepted diagnostic reference. These studies cover a wide variety of conditions such as surgical maneuvers [27-29], Valsalva straining [27], and exercise to exhaustion [30], in both adults [31] and the elderly [32].

For the purpose of this work we will assume that the measurements of finger arterial blood pressure obtained in ideal laboratory conditions using Finapres noninvasive hemodynamic monitoring system are correct and that continuous noninvasive blood pressure accurately tracks intra-arterial pressure over the short term as stated in [33].

5 Experimental Data

The validation data from human subjects were obtained under an experimental protocol approved by the Massachusetts Institute of Technology's Committee on the Use of Humans as Experimental Subjects (COUHES Approval No. 0403000233) and following Federal Regulations for the Protection of Human Subjects (45 CFR 46).

5.1 Experimental Setup

To obtain the experimental data necessary for our analysis we used a setup (Fig. 9) consisting of several components: an infrared photoplethysmographic Ring Sensor, two accelerometers, and a laptop with data acquisition board. Photoplethysmographic Ring Sensor is built of a GaAlAs high power LED emitter (PDI-E835, $\lambda = 940$ nm, Advanced Photonix Inc.), a Si PIN photodiode array (S8558, Hamamatsu), and a 5 PSI pressure sensor (EPL-B0, Entran) for providing continuous information about the circumferential pressure applied to the finger. The readings from two accelerometers (MXA2500G, MEMSIC), were placed as shown in Figure 9, and the kinematic relationship from Eq. 4.1 was used to calculate the hydrostatic pressure. The output of the photoplethysmograph sensor is pre-amplified with a standard analog amplifier and band-limited using 2^{nd} order lowpass inverting Bessel filter (cutoff frequency 30 Hz). Finapres noninvasive hemodynamic monitoring system is used to measure the arterial blood pressure for the calibration and validation purposes. All signals are sampled at 200 Hz using a 16-bit data acquisition card (NI-6036E, National Instruments), recorded, and

displayed through the graphical user interface written in Visual Studio Programming Environment (Microsoft).

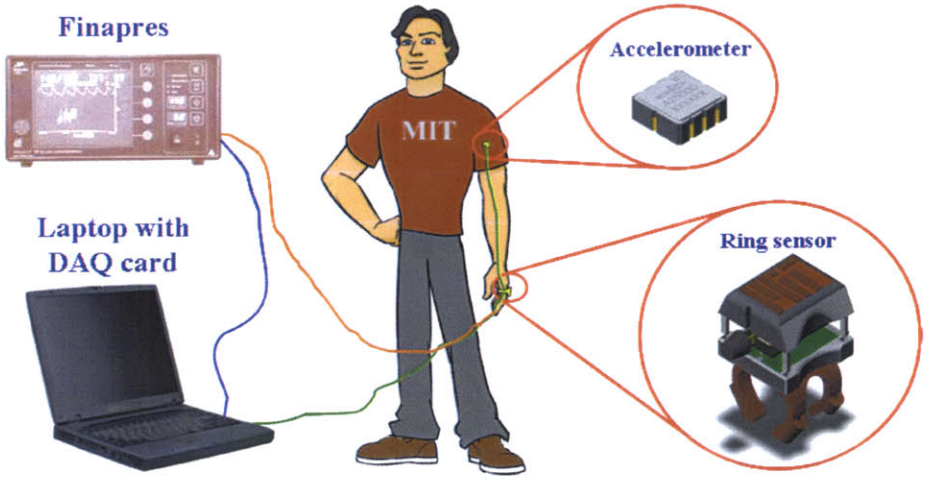

Figure 9. Schematic representation of experimental setup

5.2 Graphical User Interface

Data acquisition was performed using the graphical user interface (Fig. 10) built in Microsoft Visual Studio supported by National Instruments Measurement Studio. Microsoft Visual Studio is Microsoft's integrated development environment which allows programmers to create standalone applications running under Windows operating system. National Instruments Measurement Studio is an integrated suite of measurement and automation controls, tools, and class libraries for Visual Studio facilitating the configuration and control of the plug-in data acquisition devices produced by National Instruments.

The software is capable of selecting automatically the photodiode array channel giving the best signal using the criteria of the largest amplitude and the biggest signal to

noise ratio. This should ensure that the correct Ring Sensor placement is over a digital artery. Additionally, the software offers the possibility to select the signals which will be displayed and/or recorded guaranteeing uninterruptible data transfer, even when very high sampling frequencies are chosen.

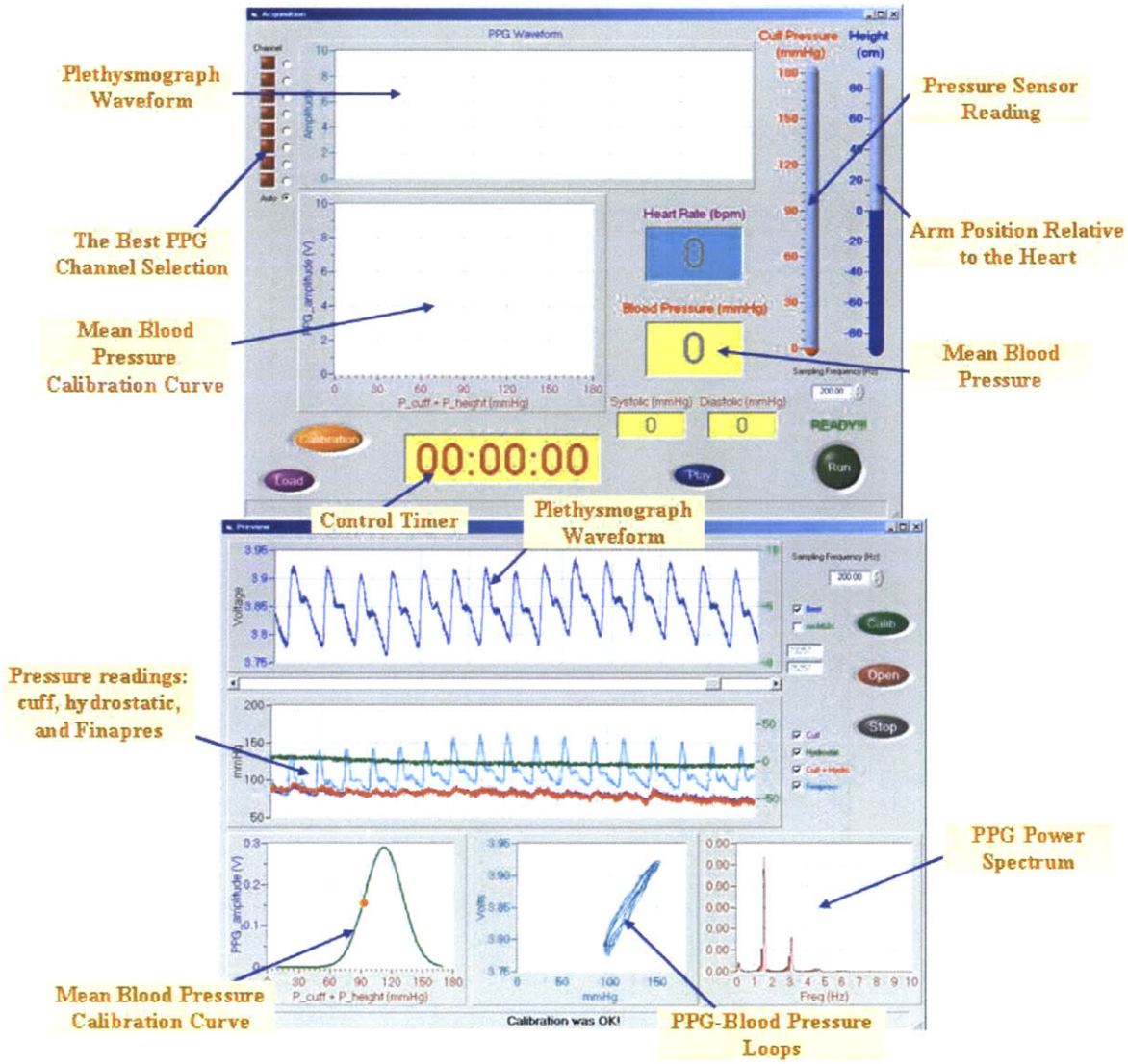

Figure 10. Windows-based graphical user interface for the Ring Sensor, the accelerometers, and the Finapres monitoring system

5.3 Protocol

A standard experimental protocol consisted of attaching the Ring Sensor to a fingerbase and the finger cuff of the Finapres blood pressure sensor to a different finger on the same hand. The instrumented arm is then placed on a platform of adjustable height and maintained at the heart level to equilibrate for ten minutes. Arm height relative to the heart is recorded using the readings from two accelerometers as described previously (Section 4.2). The micro-pressure sensor (EPL-B0, Entran) inside the Ring Sensor cuff is positioned with the diaphragm firmly over the bone of the finger.

After a rest period of approximately ten minutes, the data were acquired using the following protocol:

- The arm height was increased from 50 cm below the heart to 50 cm above the heart in increments of 15 cm for approximately 20 seconds at each height level (logically, the maximum achievable height depends on the subject's arm length).

Once acquired with sampling frequency of 200 Hz, the waveforms (PPG, pressure sensor, and sensor height signals) were recorded and processed offline as described in following section of this document.

6 Blood Pressure Waveform Reconstruction

As a proof-of-concept the experiments were performed to demonstrate the proposed approach and verify the analysis method. Nonlinear system identification was implemented to identify specify the model parameters using the experimental data obtained following the protocol described in previous section (Section 5.3). The system input was the measured transmural pressure and the output was the photoplethysmographic signal measured with a Ring Sensor. The identification was implemented in Matlab using the batch processing. Mean squared error, $V_N\left(Z^N,\theta,\eta\right)$, performance was used to assess the identified Wiener model. An iterative Gauss-Newton procedure was performed to minimize previous criterion. Usually, less then 30 iterations were needed to achieve the minimum mean squared error.

6.1 Choosing the Model

As we discussed previously, the relationship between transmural pressure and photoplethysmographic signal is nonlinear and dynamic. Therefore, we approach the problem of choosing the model on the assumption that the system can be characterized by a combination of linear dynamics and static nonlinearity at output. An experimentally obtained P_{tm} *-PPG* curve is shown in Figure 11.

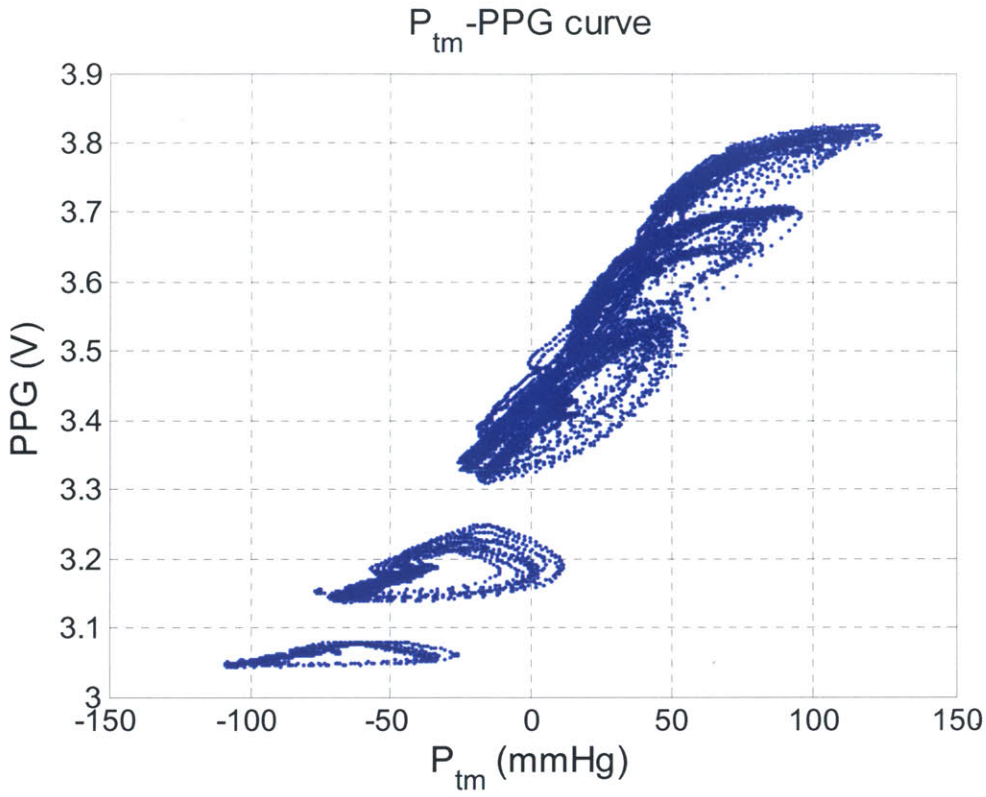

Figure 11. Experimental $P_{tm} - PPG$ curve

Linear dynamic part of a model described by Eq. 2.2 can be transformed to a discrete equivalent in the following form:

$$\frac{x(t)}{P_{tm}(t)} = \frac{\theta_1 + \theta_2 q^{-1} + \theta_3 q^{-2}}{1 + \theta_4 q^{-1} + \theta_5 q^{-2}} \tag{6.1}$$

where θ_1, θ_2, θ_3, θ_4 and θ_5 are the parameters to be identified.

Seeing that from Eq. 6.1, the linear dynamics is second order and was chosen to keep the system's complexity as low as possible. However, it is likely to add some additional first order terms such as taking into account the filtering in electrical circuitry. Yet, we know that both input and output were subjected to low pass filtering. Hence, we have assumed that the "real" process dynamics can be well described as second order.

On the other side, the static nonlinearity has been chosen to be of sigmoid type. The intuition coming from Figure 11 suggested it can be so, since the S-shaped trend is noticeable. Also, sigmoid curve resembles trends in the life-cycle of many living things and phenomena. There are a variety of sigmoid curves, but here we have used:

$$PPG(t) = \eta_1 + \frac{\eta_2}{1 + e^{-\eta_3 x(t)}} \tag{6.2}$$

where η_1, η_2 and η_3 are the parameters to be identified.

At this point, it should be noted that the model was chosen based on the discussion given in Chapter 2 of this document. It is to say, of gray-box type. However, with regards to the complexity of the system, the model can be augmented to involve more parameters. This may lead to increased accuracy of the estimates.

6.2 Implementation and Model Tuning

Because the quadratic error criterion, Eq. 3.3, cannot be minimized by analytical methods, we have done so numerically, by applying an iterative search scheme. The Gauss-Newton method was chosen because of the available computational resources and relative simplicity of implementation which was suitable for our purpose. Formulae involved in the algorithm are presented in Chapter 3. Here, we will present a brief and basic guideline of the implementation, but some detailed and explicit search schemes can be found in [13].

In order to avoid the local minima, a key question is how to choose an initial parameter estimate. Based on the chosen model we will suggest a way to select the initial

parameter values. Apparently, the final result will show a good trend for estimating the arterial blood pressure waveform from measured PPG signal.

Our approach to attain the desired parameters is summarized in the following algorithm:

Algorithm

Input: Data set $Z^N = \{P_{tm}(t);\ PPG(t)\}_{t=1}^{N} = \{u(t);\ y(t)\}_{t=1}^{N}$

Output: Parameter estimates $\hat{\theta}$ and $\hat{\eta}$ giving $H(q;\hat{\theta})$, the linear dynamic system, and $f(.,\hat{\eta})$, the static nonlinearity.

Initial parameter estimates:

Step 1: Parameterize the linear system by means of an ARX model,

$$x(t) = -\theta_4 x(t-1) - \theta_5 x(t-2) + \theta_1 u(t) + \theta_2 u(t-1) + \theta_3 u(t-2)$$

with a parameter vector $\theta^T = [\theta_1 \quad \theta_2 \quad \theta_3 \quad \theta_4 \quad \theta_5]$

Step 2: Assume $x(t) = y(t)$ and use linear regression to find initial estimate of parameters $\theta_1, \theta_2, \theta_3, \theta_4$ and θ_5. Normalize an initial transfer function to be with unit DC gain.

Step 3: Write static nonlinearity in form $y(t) = \eta_1 + \frac{\eta_2}{1 + e^{-\eta_3 x(t)}}$ (It is important that the function is invertible. Certainly, sigmoid function in this form is invertible.) The parameter vector for the sigmoid is $\eta^T = [\eta_1 \quad \eta_2 \quad \eta_3]$

Step 4: Assuming $x(t) = u(t)$ perform **nonlinear fit** to make an initial estimate of the parameters η_1, η_2 and η_3.

Prediction error criterion and minimization:

Step 5: Formulate the quadratic error criterion

$$V_N(Z^N,\theta,\eta)=\frac{1}{N}\sum_{t=1}^{N}(PPG(t)-y_{PPG}(t\mid\theta,\eta))^2$$

Step 6: Solve the resulting optimization problem using **Gauss-Newton minimization** as a way to numerically find the values of θ and η that minimize the squared error

$$(\hat{\theta}_N,\hat{\eta}_N)=\underset{\theta,\eta}{arg\,min}\,V_N(Z^N,\theta,\eta)$$

Step 7: Now it is easy to write inverse model

$$u(t)=f^{-1}(y(t))$$

Step 8: Reconstruct the ABP waveform from PPG input and measured hydrostatic pressure.

There is no general rule for choosing the initial parameter values. In our case the results obtained using the Steps 2 and 4 of previous algorithm were satisfactory, leading to a small number of iterations and a small final criterion value.

As noted in [14] the Wiener model is over-parameterized if the linear and nonlinear subsystem are parameterized separately. Numerical problems will occur if the over-parameterization is not addressed, because a constant gain can be distributed arbitrarily between the subsystems. Therefore, a simple way to get a unique solution is just to fix one of the parameters of the linear system, and allow it be constant during the minimization. In our case, we fixed the parameter θ_1 to value 1 to ensure that the denominator of the inverse linear system is monic.

To test the validity of previous algorithm, we began our experiments and recorded the signals from the PPG Ring Sensor, the accelerometers, the pressure sensor, and the Finapres. Figure 12 shows the acquired waveforms (approximately 90 seconds). Upper plot shows the PPG waveform. Down plot shows the hydrostatic pressure (dark green), the pressure from pressure sensor (red), and from Finapres (light green), and calculated transmural pressure (blue). The signals were low pass filtered using a 2nd order digital Butterworth filter with a cut-off frequency of 30 Hz. The PPG and transmural pressure data vs. time presented in Figure 12 are the same ones shown in Figure 11.

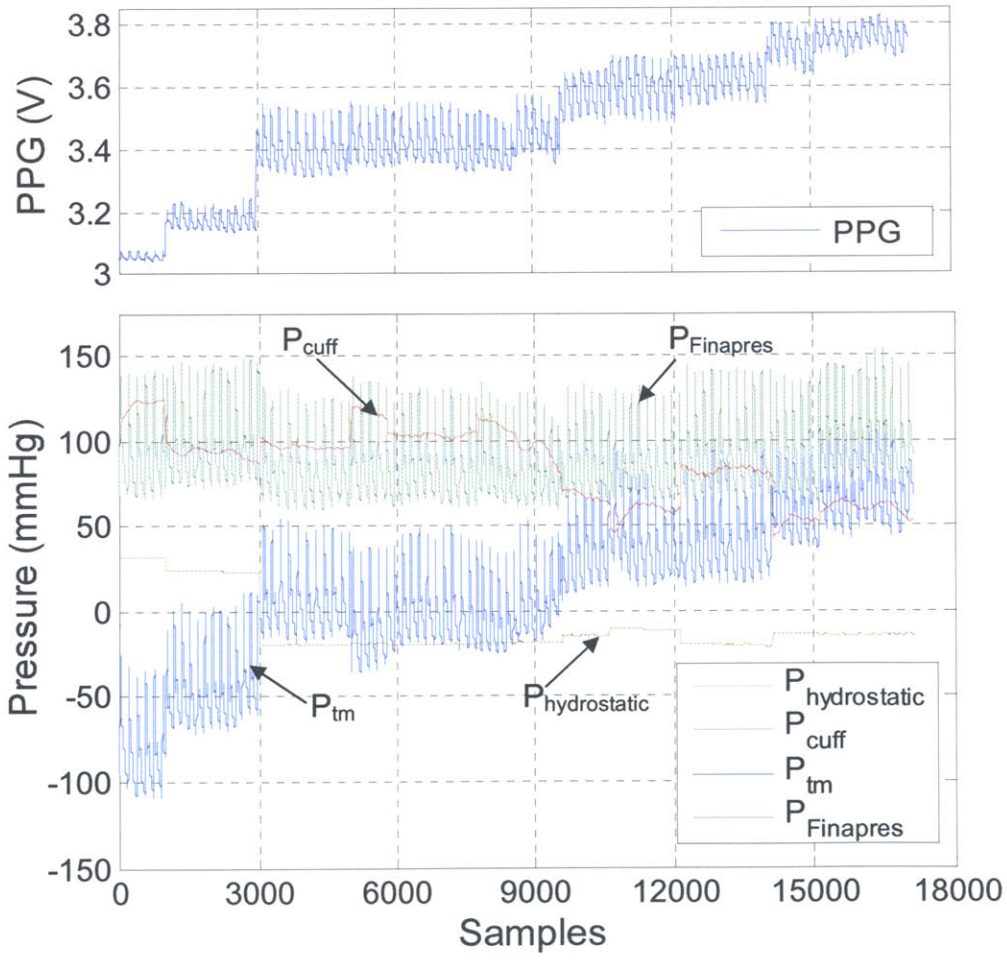

Figure 12. Experimental waveforms: PPG obtained from the Ring Sensor (up); Finapres blood pressure, hydrostatic pressure calculated from accelerometers' readings, pressure sensor signal, P_{cuff} (down)

The data set was formed and the identification algorithm was applied. Initial parameter estimates for the linear dynamic part were:

$$\theta^T = [0.0144 \quad -0.0241 \quad 0.0097 \quad -1.5548 \quad 0.5548]$$

and for the static nonlinearity:

$$\eta^T = [2.9808 \quad 0.9632 \quad 0.0247]$$

obtained in the way suggested in steps 2 and 4 from the algorithm. Figure 13 shows the system identification results. Upper plot shows a simulated PPG signal (blue) and measured PPG signal (green) over approximately 90 seconds. Lower left plot illustrates estimated sigmoid (red) and estimated output of the linear dynamic part (green). Finally, lower right plot shows how the value of prediction error criterion changed through the iterations. The prediction error criterion value was 0.001127, achieved after 19 iterations. Identified parameter values were:

$$\theta_N^T = [1.0000 \quad -1.4525 \quad 0.4827 \quad -0.4348 \quad -0.5298]$$

and,

$$\eta_N^T = [2.8849 \quad 1.1055 \quad 0.0247]$$

Here, it is important to note the relevance of using a large number of decimals in parameter value. This significantly increases the precision of the calculations and it is one of the key characteristics of discrete systems. Because of the compactness of parameter vector form, we have used just four decimal places.

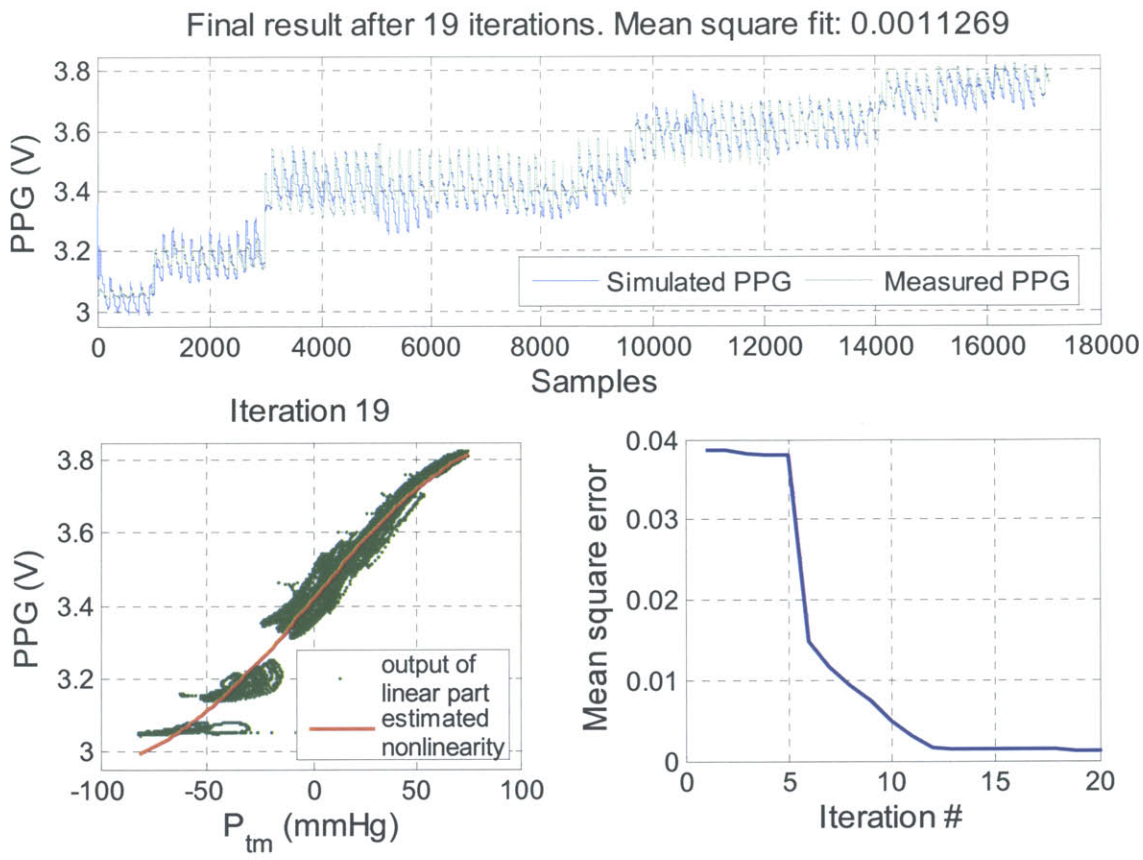

Figure 13. System identification results: up – measured PPG waveform (blue) and estimated PPG waveform after a final iteration (green); down left – estimated sigmoid (red) and estimated output of the linear dynamic part (green); down right – prediction error criterion value vs. iteration number

The result of waveform estimation was satisfactory. Figure 14 shows a part of measured PPG waveform (green) and the ability of the identified model to reproduce it (blue). The mismatches in some portions of the waveform may be caused by a time-varying nature of the signal and the disturbances to the system. Certainly, the motion artifact, respiration and other physiological effects will contribute to the final result and these factors should be taken into account, especially due to the change in arm position. Also, as mentioned previously, the complexity of the system can be described more precisely with additional parameters. However, that would increase the computational

cost and limit the applicability. Overall, both signals show an excellent match which validate our approach.

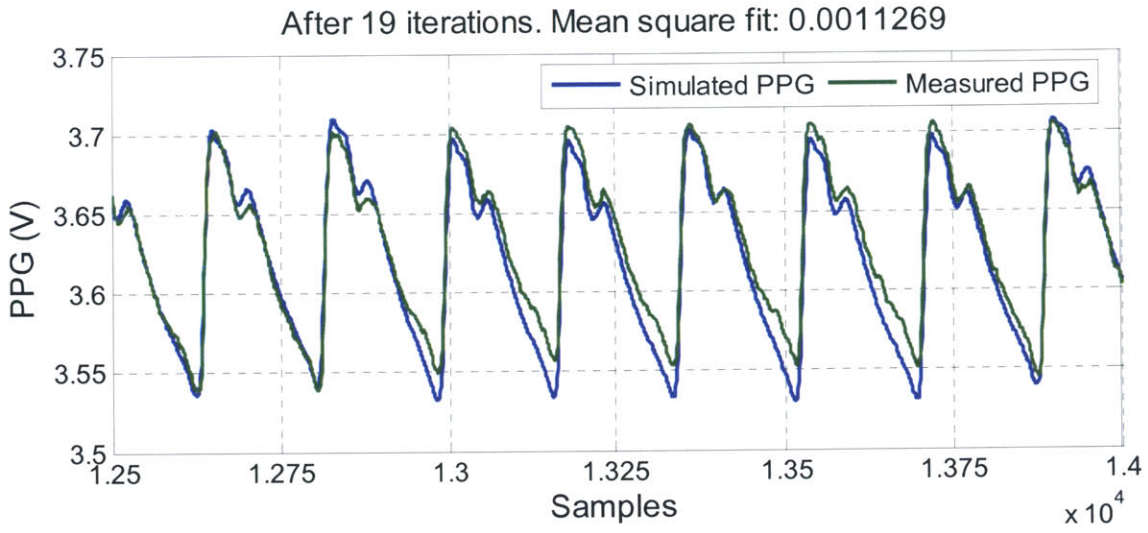

Figure 14. Simulated PPG waveform

6.3 Estimation of Arterial Blood Pressure Waveform

Our final goal has been to reconstruct the arterial blood pressure waveform using a model tuned from the procedure described in previous section and **only** the signals obtained from the wearable Ring Sensor (including the accelerometers and the pressure sensor). Having identified the parameters and by simply inverting the linear and nonlinear subsystems of the Wiener model, the blood pressure waveform can be estimated.

Figure 15 shows a representative section of experimentally obtained signals from a human subject which are used to estimate the arterial blood pressure: PPG signal (blue), hydrostatic pressure relative to the heart level (green), and applied external pressure (red).

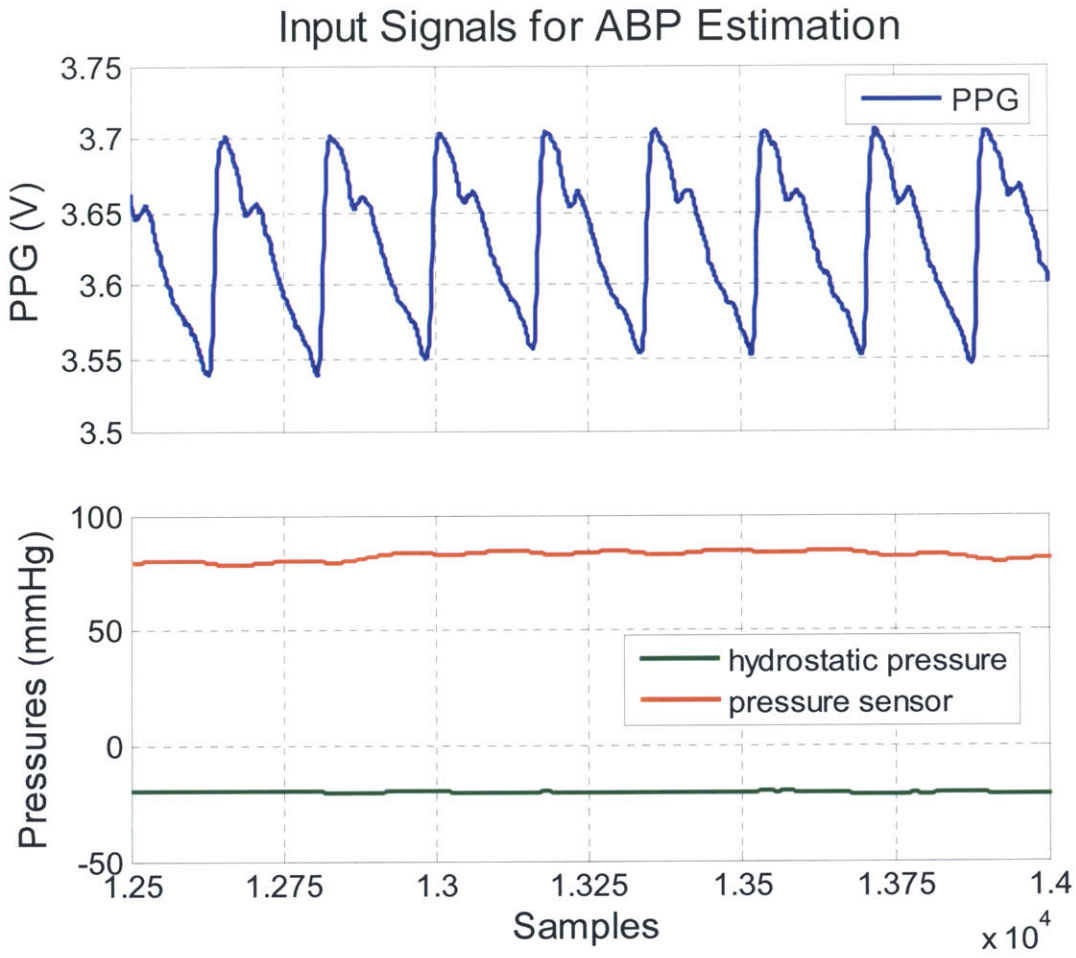

Figure 15. Input signals for arterial blood pressure waveform reconstruction: a part of PPG waveform (up);the sections of hydrostatic pressure and pressure sensor signal (down)

The input to the model is the PPG signal, passing through an inverse of sigmoid nonlinearity and giving an intermediate signal, $x(t)$:

$$x(t) = -\frac{1}{\eta_3} ln\left(\frac{\eta_2}{PPG(t) - \eta_1} - 1\right) \tag{6.3}$$

where η_1, η_2 and η_3 are the parameters identified. The intermediate signal $x(t)$ should pass through the inverse linear dynamic model of that one given with Eq. 6.1 producing an estimate of transmural pressure, $P_{tm}(t)$:

$$P_{tm}(t) = \frac{1}{\theta_1}\left[x(t) + \theta_4 x(t-1) + \theta_5 x(t-2) - \theta_2 P_{tm}(t-1) - \theta_3 P_{tm}(t-2)\right] \tag{6.4}$$

where θ_1, θ_2, θ_3, θ_4 and θ_5 are the parameters identified earlier. Eq. 6.4 has been simply implemented as a filter in Matlab. In our system we fixed the parameter θ_1 with value 1 in order to ensure that the denominator of inverse linear transfer function was monic. Also, through the Gauss-Newton iterations, care was taken to ensure that the inverse linear transfer function was stable, by mapping eventually unstable poles inside the unit circle. Figure 16 shows a representative part of the estimated transmural pressure waveform (blue) as a "byproduct" of ABP waveform reconstruction, and the measured waveform (green).

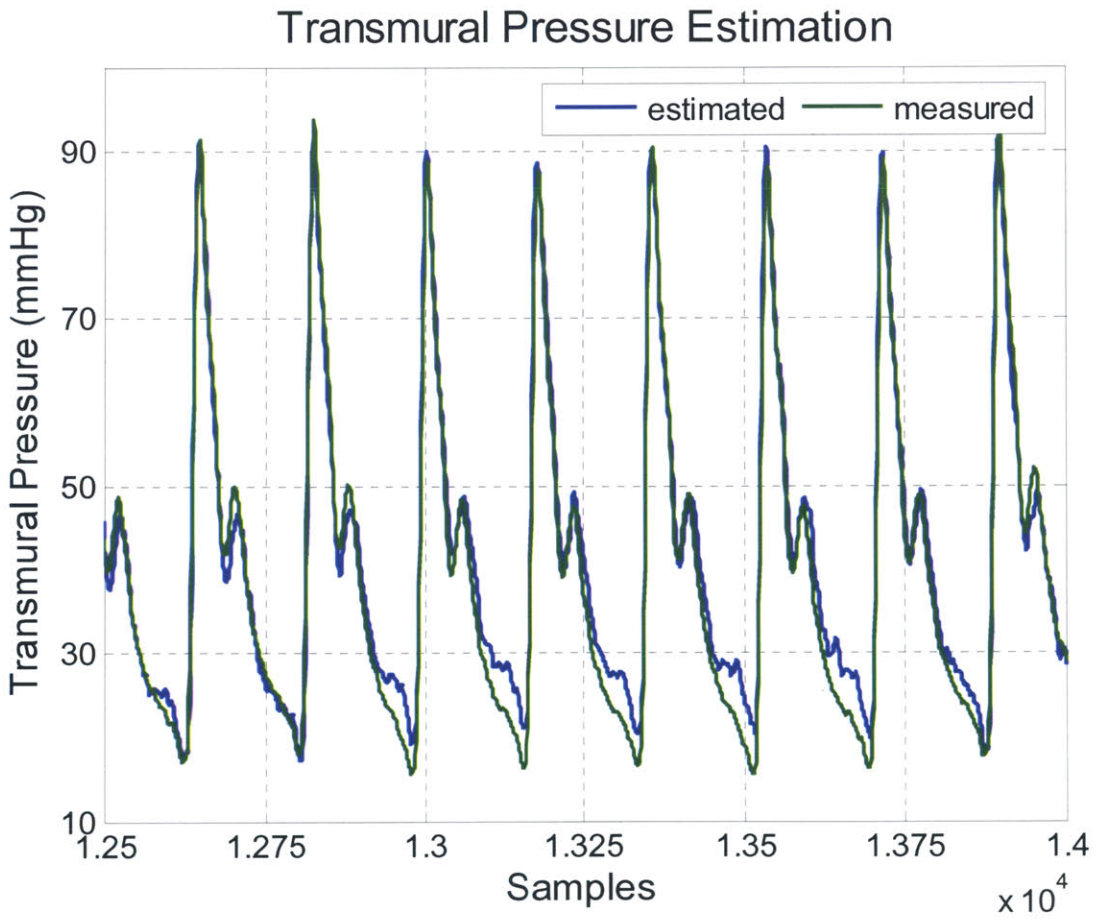

Figure 16. A reconstructed piece of transmural pressure waveform

As mentioned before, the blood pressure in digital artery, P_{ABP}, is related to transmural pressure as:

$$P_{ABP} = P_{tm} - \rho g h + P_{external} \tag{6.5}$$

where all variables are defined in Chapter 2. Now, having all these variables measured, or estimated, it is easy to calculate the arterial blood pressure from Eq. 6.5. The reconstructed ABP waveform is shown in Figure 17 (blue), together with the waveform measured with Finapres (green). Although the systolic and diastolic points were slightly overestimated, the general trend in anacrotic and dicrotic limbs showed a remarkable agreement with the ABP measured with Finapres.

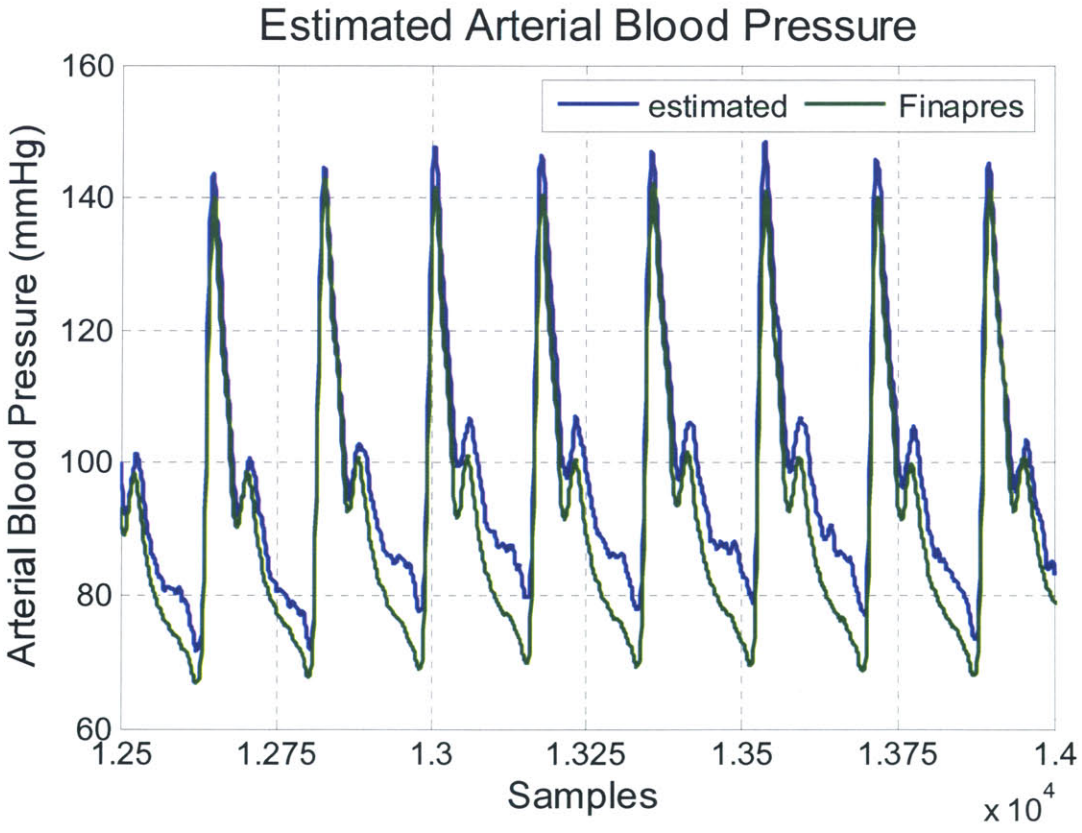

Figure 17. A reconstructed segment of finger arterial blood pressure waveform

7 Conclusions

7.1 Summary of Contributions

A new system identification algorithm has been developed to reconstruct an arterial blood pressure waveform using the signals obtained from a wearable photoplethismographic Ring Sensor and an Arm Accelerometer Sensor.

Based on nonlinear dynamic viscoelastic properties of arterial wall a simple nonlinear Wiener model structure has been used successfully to represent transmural preesure-volume relationship in artery.

A novel iterative algorithm has been developed to directly identify the parameters of chosen Wiener model, including the method to provide the initial parameter estimates, which is a key to a successful system identification procedure. Also, it has been ensured that the inverse linear dynamic part of the model was stable and its denominator was monic.

Transmural pressure range has been scanned experimentally by inducing hydrostatic pressure variations about a datum point at the heart level. Those variations have been estimated using a kinematic relationship and measuring the tilt of the Arm Accelerometer Sensor's axes.

The Wiener model structure identification was applied experimentally with data obtained from a human subject. The resulting trend in estimated ABP waveform showed an excellent agreement with the measurements acquired from the gold standard device.

7.2 Future Work

There are several limitations that must be addressed prior to the application of this methodology for a wearable sensing device used in arterial blood pressure measurement.

The model can be improved to capture the waveform features more accurately. Because, the linear and nonlinear subsystem are parameterized separately the Wiener model is over-parameterized. Numerical problems will occur if the over-parameterization is not addressed and it is necessary to deal efficiently with distribution of a constant gain between the subsystems.

The system identification procedure uses a Gauss-Newton method. This algorithm has slow convergence close to the local minimum point. Thus, the identification procedure can be speed up by implementing some numerical search scheme other then Gauss-Newton algorithm. This is important, especially, if one thinks about "real-time" parameter identification in a device for ABP measurement.

The performance of the identification algorithm should be further verified using the data from a larger sampling pool. Moreover, the non bias selection of subjects should cover a variety of characteristics, such as differences in height, differences in age, and gender differences as well. Also, the variety of healthy conditions will be very useful to validate further the methodology and also extend it to assess disease state.

8 References

[1] E. P. Widmaier, H. Raff, and K. T. Strang, *Vander's human physiology: the mechanisms of body function*, 10 ed. Boston: McGraw-Hill, 2006.

[2] M. F. O'Rourke and T. Yaginuma, "Wave reflections and the arterial pulse," *Arch Intern Med*, vol. 144, pp. 366-71, 1984.

[3] G. O. Darovic, *Hemodynamic Monitoring: Invasive and Noninvasive Clinical Application. 2nd ed.* Philadelphia, Pa: WB Saunders Co, 1995.

[4] Y. C. Fung, *Biomechanics: mechanical properties of living tissues*. New York: Springer-Verlag, 1981.

[5] A. Guyton and J. Hall, *Textbook of Medical Phisiology*, 9th ed ed. Philadelphia: W.B. Saunders Company, 1996.

[6] D. Roylance, "Engineering Viscoelasticity," in *3.11 Mechanics of Materials*. Cambridge, MA: MIT OpenCourseWare, 2001.

[7] G. J. Langewouters, A. Zwart, R. Busse, and K. H. Wesseling, "Pressure-diameter relationships of segments of human finger arteries," *Clinical physics and physiological measurement*, vol. 7, pp. 43-56, 1986.

[8] J. Penaz, "Photoelectric measurement of blood pressure, volume and flow in the finger," in *Digest of the International Conference on Medicine and Biological Engineering*. Dresden: Dresden Conference Committee of the 10th International Conference on Medicine and Biological Engineering, 1973, pp. 104.

[9] K. H. Wesseling, B. de Wit, J. J. Settles, and W. H. Klaver, "On the indirect registration of finger blood pressure after Penaz," *Funkt Biol Med*, pp. 1245-50, 1982.

[10] I. W. Hunter and M. J. Korenberg, "The identification of nonlinear biological systems: Wiener and Hammerstein cascade models," *Biological cybernetics*, vol. 55, pp. 135-44, 1986.

[11] J. E. Dennis and R. B. Schnabel, *Numerical methods for unconstrained optimization and nonlinear equations*. Englewood Cliffs, N.J.: Prentice-Hall, 1983.

[12] D. G. Luenberger and D. G. Luenberger, *Linear and nonlinear programming*, 2nd ed. Reading, Mass.: Addison-Wesley, 1984.

[13] L. Ljung, *System identification: theory for the user*, 2nd ed. Upper Saddle River, NJ: Prentice Hall PTR, 1999.

[14] A. Hagenblad, "Aspects of the Identification of Wiener Models," in *Division of Automatic Control, Department of Electrical Engineering*, vol. Ph.D. Linkoping, Sweden: Linkopings universitet, 1999.

[15] J. Sjoberg, "On estimation of nonlinear black-box models: How to obtain a good initialization," presented at IEEE Workshop in Neural Networks for Signal Processing, Amelia Island Plantation, 1997.

[16] D. David, E. L. Michelson, and L. S. Dreifus, "Ambulatory Monitoring of the Cardiac Patients." Philadelphia: F. A. Davis Company, 1988, pp. Chapter 1.

[17] B. P. McGrath, "Ambulatory blood pressure monitoring," *The Medical journal of Australia*, vol. 176, pp. 588-92, 2002.

[18] "http://www.finapres.com/customers/finometer.php."

[19] "http://www.finapres.com/customers/portapres.php."

[20] K. J. Fleckenstein, "The Mosso plethysmograph in 19th-century physiology," *Medical instrumentation*, vol. 18, pp. 330-1, 1984.

[21] K. Shelley and S. Shelley, "Pulse Oximeter Waveform: Photoelectric Plethysmography," in *Clinical Monitoring*, C. Lake, R. Hines, and C. Blitt, Eds.: W.B. Saunders Company, 2001, pp. 420-428.

[22] K. H. Wesseling, B. de Wit, G. M. A. van der Hoeven, J. van Goudoever, and J. J. Settels, "Physiocal, Calibrating Finger Vascular Physiology for Finapres," *Homeostasis In Health and Disease*, vol. 36, pp. 67-82, 1995.

[23] S. Rhee and Massachusetts Institute of Technology. Dept. of Mechanical Engineering., "Design and analysis of artifact-resistive finger photoplethysmographic sensors for vital sign monitoring," 2000, pp. 101 leaves.

[24] S. Rhee, B.-H. Yang, and H. Asada, "The Ring Sensor: a New Ambulatory Wearable Sensor for Twenty-Four Hour Patient Monitoring," presented at 20th Annual International Conference of the IEEE Engineering in Medicine and Biology Society, Hong Kong, Oct, 1998.

[25] B.-H. Yang, S. Rhee, and H. Asada, "A Twenty-Four Hour Tele-Nursing System Using a Ring Sensor," presented at 1998 IEEE International Conference on Robotics and Automation, Leuven, Belgium, May, 1998.

[26] P. Shaltis, A. Reisner, and H. Asada, "Wearable, Cuff-less PPG-Based Blood Pressure Monitor with Novel Height Sensor," presented at 28th Annual International Conference of the IEEE/EMBS, New York, New York, 2006.

[27] B. P. Imholz, G. A. van Montfrans, J. J. Settels, G. M. van der Hoeven, J. M. Karemaker, and W. Wieling, "Continuous non-invasive blood pressure

monitoring: reliability of Finapres device during the Valsalva manoeuvre," *Cardiovascular research*, vol. 22, pp. 390-7, 1988.

[28] N. T. Smith, K. H. Wesseling, and B. de Wit, "Evaluation of two prototype devices producing noninvasive, pulsatile, calibrated blood pressure measurement from a finger," *Journal of clinical monitoring*, vol. 1, pp. 17-29, 1985.

[29] J. van Egmond, M. Hasenbos, and J. F. Crul, "Invasive v. non-invasive measurement of arterial pressure. Comparison of two automatic methods and simultaneously measured direct intra-arterial pressure," *British journal of anaesthesia*, vol. 57, pp. 434-44, 1985.

[30] R. N. Idema, A. H. van den Meiracker, B. P. Imholz, A. J. Man in 't Veld, J. J. Settels, H. J. Ritsema van Eck, and M. A. Schalekamp, "Comparison of Finapres non-invasive beat-to-beat finger blood pressure with intrabrachial artery pressure during and after bicycle ergometry," *Journal of hypertension. Supplement*, vol. 7, pp. S58-9, 1989.

[31] G. Parati, R. Casadei, A. Groppelli, M. Di Rienzo, and G. Mancia, "Comparison of finger and intra-arterial blood pressure monitoring at rest and during laboratory testing," *Hypertension*, vol. 13, pp. 647-55, 1989.

[32] W. J. W. Bos, "Measurement of finger and brachial artery pressure." University of Amsterdam: Amsterdam, The Netherlands, 1995.

[33] J. K. Triedman and J. P. Saul, "Comparison of intraarterial with continuous noninvasive blood pressure measurement in postoperative pediatric patients," *Journal of clinical monitoring*, vol. 10, pp. 11-20, 1994.